New diagnostic tools for transport measurements in the scrape-off layer (SOL) of medium-size tokamaks

Schneider, B. S.; Ionita, C.; Costea, S.; Vasilovici, O.; Kovačič, J.; Gyergyek, T.; Končar, B.; Draksler, M.; Nem, R. D.; Naulin, V.

Total number of authors:
16

Published in:
Plasma Physics and Controlled Fusion

Link to article, DOI:
10.1088/1361-6587/ab0596

Publication date:
2019

Document Version
Publisher's PDF, also known as Version of record

Plasma Physics and Controlled Fusion

PAPER • **OPEN ACCESS**

New diagnostic tools for transport measurements in the scrape-off layer (SOL) of medium-size tokamaks

To cite this article: B S Schneider *et al* 2019 *Plasma Phys. Control. Fusion* **61** 054004

OPEN ACCESS
IOP Publishing
Plasma Physics and Controlled Fusion
Plasma Phys. Control. Fusion **61** (2019) 054004 (12pp)
https://doi.org/10.1088/1361-6587/ab0596

New diagnostic tools for transport measurements in the scrape-off layer (SOL) of medium-size tokamaks*

B S Schneider[1], C Ionita[1,8], S Costea[1], O Vasilovici[1], J Kovačič[2], T Gyergyek[2,3], B Končar[2], M Draksler[2], R D Nem[4], V Naulin[4], J J Rasmussen[4], M Spolaore[5], N Vianello[5], R Stärz[6], A Herrmann[7] and R Schrittwieser[1]

[1] Institute for Ion Physics and Applied Physics, University of Innsbruck, Austria
[2] Jožef Stefan Institute, Ljubljana, Slovenia
[3] Faculty of Electrical Engineering, University of Ljubljana, Slovenia
[4] Department of Physics, Technical University of Denmark, Kgs. Lyngby, Denmark
[5] Consorzio RFX, Padua, Italy
[6] Mechatronic Department, Management Center Innsbruck. Innsbruck, Austria
[7] Max-Planck-Institute for Plasma Physics, Garching near Munich, Germany

E-mail: codrina.ionita@uibk.ac.at

Received 4 November 2018, revised 15 January 2019
Accepted for publication 8 February 2019
Published 21 March 2019

Abstract

We present a new diagnostic tool for the determination of various plasma parameters in the edge region of medium-size tokamaks (MST) and stellarators (specifically Wendelstein 7-X) which is under development under the EUROfusion project task force MST2 and S1. This will be a probe head (called the new probe head-NPH) which will carry two cold Langmuir probes, one electron-emissive probe (EEP), two retarding field analysers (RFA) facing upstream and downstream and two magnetic pickup coils. By various adaptors, the same NPH will be used on all three European MSTs (ASDEX Upgrade, TCV and MAST-U) and on Wendelstein 7-X. For the first time the plasma potential in the edge region of MSTs and comparable toroidal fusion experiments will be directly determined by an EEP that will be permanently heated during the measurements. After the introduction and the theoretical background especially of the EEP, the NPH and its components are described in detail. The NPH will be able to measure electron and ion temperature, electron and ion density, cold floating potential, plasma potential and magnetic fluctuations in all three directions of space at two radial positions.

Keywords: plasma diagnostics, plasma probes, probe head, turbulence edge transport

(Some figures may appear in colour only in the online journal)

1. Introduction

Understanding turbulence in the edge region of toroidal magnetised plasmas is one of the key issues in modern fusion research. Great experimental and theoretical efforts are devoted to understand and quantify radial particle and energy losses and radial transport of poloidal momentum (see e.g. [2–4]). This transport is dominantly turbulent and intermittent and is mainly caused by strong filamentary structures originating from the edge of magnetically confined plasmas. They

* See reference [1]
[8] Author to whom any correspondence should be addressed

become elongated along the magnetic field and propagate radially towards the chamber walls. These structures are observed in both low-confinement and high-confinement modes (L- and H-mode) of tokamaks and are referred to as plasma blobs. Also in stellarators such phenomena have been observed (see e.g. [5–7]).

Comprehensive and accurate investigations of blobs require diagnostics which can measure several parameters simultaneously, locally and with high temporal resolution. The most important parameters are plasma potential, Φ_{pl}, electron and ion temperature, $T_{e,i}$, and electron and ion densities, $n_{e,i}$. For the determination of Φ_{pl}, T_e and n_e the best suited diagnostic tools are plasma probes [8, 9]. However, conventional cold Langmuir probes (CLP) are not sufficient, primarily since Φ_{pl} and T_e can only be derived indirectly from the current–voltage characteristics and thus with low temporal resolution. While Φ_{pl} can in principle also be derived from the floating potential, V_{fl}, of a CLP, this is also of no avail since the difference between V_{fl} and Φ_{pl} depends on T_e [10–14] (see below). The electron temperature has, however, strong gradients and fluctuations especially in the edge region of magnetised toroidal plasmas and cannot be determined with sufficient accuracy and good temporal resolution.

We have developed probes whose floating potential is close, or ideally equal to Φ_{pl}, so that this important parameter can be measured directly and thus with high temporal resolution [14]. Such plasma potential probes (PPP) are either electron-emissive probes (EEP), operable in all types of plasma [13, 15], or electron screening probes (ESP) drawing on the difference of the gyroradii of electrons and ions in magnetic fields [12, 16, 17]. In both cases the floating potential $V_{fl,ppp}$ of such probes is a good approximation of the plasma potential [14]. With arrays of PPPs, electric field components can be determined with much higher reliability than with CLP since $V_{fl,ppp}$ does ideally not depend on T_e. On the other hand, from the difference between the floating potential of a CLP and the plasma potential the electron temperature can be determined (see below). This can be realised by one CLP and one PPP mounted closely by each other on one probe head. More details on the EEP and the ESPs developed recently in our group will be presented in forthcoming papers [13, 14].

For comprehensive investigations of blobs in the edge region of toroidal magnetic fusion experiments a new probe head (NPH) has been developed which combines two CLPs, an EEP and two retarding field analysers (RFA) for ion energy distribution measurements [18–20]. The NPH also carries two magnetic pickup coils (MPC) to measure magnetic field fluctuations on two radial positions [21, 22]. The NPH will be robust enough to withstand the strong plasma heat and particle fluxes in the edge regions of toroidal magnetic fusion experiments and will make it possible to simultaneously measure plasma potential, electron and ion temperature, electron and ion density and magnetic fluctuations.

In this research note the NPH will be described which will be used in all three present European medium-size tokamaks (MST) for comparative measurements of transport parameters:

1. Tokamak à configuration variable (TCV) at the Swiss Plasma Center (SPC) of the École Polytechnique Fédérale de Lausanne in Lausanne, Switzerland [23].
2. ASDEX Upgrade (Axial-Symmetric Divertor EXperiment—AUG) at the IPP (Max-Planck Institute for Plasma Physics) in Garching near Munich, Germany [24].
3. Mega-Ampere Spherical Tokamak (MAST-U) at the Culham Centre for Fusion Energy in Culham, UK [25].

Also in Wendelstein 7-X of the Max-Planck-Institute for Plasma Physics in Greifswald, Germany, [26] the application of the NPH is envisaged to compare the measurements of transport parameters with those of MSTs.

To avoid mounting and dismounting the same NPH on the various probe manipulators of the three MSTs and the Wendelstein 7-X, several identical probe heads will be constructed and employed. In AUG two NPHs will be employed and operated simultaneously, one on the mid-plane manipulator (MEM—from German 'Mittel-Ebenen-Manipulator'), and one on the X-point reciprocator (XPR).

2. Theoretical considerations

Whereas (cold) probes were used in plasmas even long before the famous works by Mott–Smith and Langmuir [8, 9, see also 14], until about the end of last century they were employed almost exclusively in laboratory plasmas and small toroidal fusion experiments; all these probes were what we now conveniently call CLPs. Due to the much higher plasma temperatures, the use of probes in MST and larger stellarators with typical discharge lengths of several seconds has long been considered hardly feasibly since the probes would be damaged and destroyed quickly. Moreover, the sputtered-off or evaporated probe material will subsequently contaminate the plasma and/or might deposit on other plasma-facing components (PFCs) possibly leading to undesirable leakage currents or even short circuits.

However, the application of probe manipulators made it possible to use probes at least in the edge region of toroidal fusion experiments, mainly in the scrape-off layer (SOL) up to almost the last closed flux surface largely without these detrimental effects. To increase the versatility it has become customary to combine several probes on so-called probe heads (see e.g. [4, 27–31]). By mounting the probe heads on manipulators the heads are then inserted into the SOL for several strokes of about 100 ms at most each time during one discharge.

Although Langmuir has also used EEPs already [32] their use was even more restricted to special applications in laboratory plasmas. Only recently EEPs were also found useful in small tokamaks [10, 33], while now they are envisaged also for MSTs. For more information on CLPs and EEPs see [13, 14].

2.1. CLPs versus EEP

In this section we would like to give a brief summary of the most important features and equations relevant for CLPs and EEPs.

For a CLP the basic, simplified relation between its floating potential $V_{\mathrm{fl,cp}}$ and the plasma potential Φ_{pl} reads [10, 13, 14, 33]:

$$V_{\mathrm{fl,cp}} = \Phi_{\mathrm{pl}} - \ln\left(\frac{|I_{\mathrm{es}}|}{|I_{\mathrm{is}}|}\right)\frac{T_{\mathrm{e}}}{e}. \tag{1}$$

Here I_{es} and I_{is} are the electron and ion saturation currents, respectively, impinging from the plasma onto the probe, T_{e} is electron temperature in energy units and e is the electron charge (T_{i} will be the ion temperature). Since in almost all types of plasmas $I_{\mathrm{es}} \gg I_{\mathrm{is}}$, inevitably $V_{\mathrm{fl,cp}} < \Phi_{\mathrm{pl}}$, and the difference between $V_{\mathrm{fl,cp}}$ and Φ_{pl} depends also on T_{e} [10, 12, 14]. This dependence can be circumvented if we succeed to make the second term of equation (1) zero, i.e. if we make the argument of the logarithm one. This goal can be reached by adding a current to the ion probe current I_{is} until numerator and denominator of the argument of the logarithm are equal in magnitude. This can be achieved by an electron emission current I_{em} from the probe into the plasma since such a current will have the same sign as I_{is}. Equation (1) for the floating potential $V_{\mathrm{fl,em}}$ of an EEP will then read:

$$V_{\mathrm{fl,em}} = \Phi_{\mathrm{pl}} - \ln\left(\frac{|I_{\mathrm{es}}|}{|I_{\mathrm{is}} + I_{\mathrm{em}}|}\right)\frac{T_{\mathrm{e}}}{e}. \tag{2}$$

Hence, if we accomplish the equality

$$|I_{\mathrm{em}} + I_{\mathrm{is}}| = |I_{\mathrm{es}}| \tag{3}$$

we have reached our goal:

$$V_{\mathrm{fl,em}} = \Phi_{\mathrm{pl}}. \tag{4}$$

Since I_{is} is almost negligible compared to I_{es}, this means that the magnitude of the emission current I_{em} must be almost as large as that of I_{es}.

This derivation is simplified insofar as we have neglected the possible formation of space charges in front of an EEP [34]. There is an ongoing discussion on the question whether a strongly emitting EEP can really float on the plasma potential, but a detailed treatment of an EEP lies beyond the scope of this paper (see our forthcoming paper [13, 14]). A discussion of the limits and restrictions of this simplified derivation and the requirements for its usage in SOL plasmas can be found in [13, 14, 33].

In a realistic experiment the procedure to verify that the emission current is sufficient for shifting $V_{\mathrm{fl,em}}$ as close as possible to Φ_{pl} is to measure $V_{\mathrm{fl,em}}$ as function of the EEP heating power P_{heat}. It is very helpful that for increasing heating power the transition from the cold floating potential V_{fl} towards Φ_{pl} (being more positive than V_{fl} by a few time T_e—equation (1)) is usually rather abrupt and that above a certain value of P_{heat} the value of $V_{\mathrm{fl,em}}$ almost saturates (see for instance [10, 30, 35, 36]). Also figure 1 illustrates the rather abrupt transition of the floating potential of an unheated, or only slightly heated EEP from that of a CLP

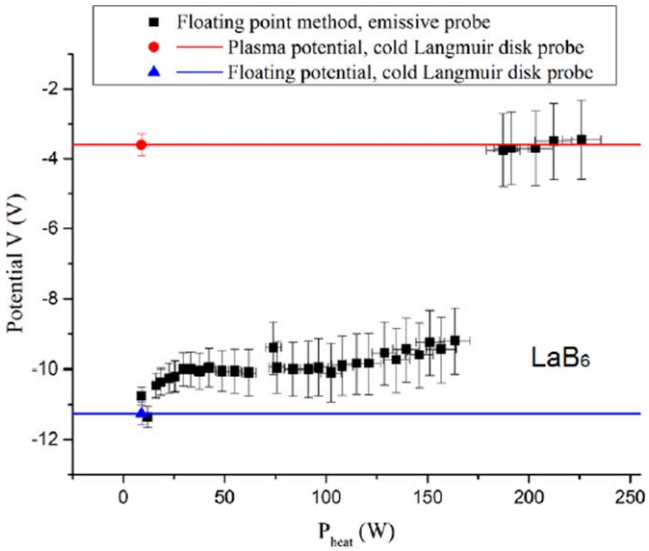

Figure 1. Typical behaviour of the floating potential $V_{\mathrm{fl,em}}$ of an EEP versus heating power P_{heat}. The blue horizontal line shows the floating potential of the unheated EEP (which therefore acts as a conventional CLP), the red horizontal line shows the value of the plasma potential determined from the current–voltage characteristic of the unheated EEP.

(horizontal blue line) to that of an EEP, being close to the plasma potential Φ_{pl} (horizontal red line). This result was obtained with an EEP similar as that one shown below in figure 2, however with a tip of LaB_6, in an unmagnetized argon plasma with a density of approximately 10^{17} m^{-3} and an electron/ion temperature of around 2 eV/0.2 eV [37].

Above the threshold of P_{heat} (which in case of figure 1 is around 175 W) the actual value of the heating power is therefore not very critical since $V_{\mathrm{fl,em}}$ remains constant very close, or even slightly above Φ_{pl} [38]. Hence for the determination of spatial or temporal variations of $V_{\mathrm{fl,em}} \cong \Phi_{\mathrm{pl}}$ it suffices to adjust P_{heat} at a sufficiently high value above the threshold.

We would like to point out that if we have the possibility to measure the floating potential $V_{\mathrm{fl,cp}}$ of a CLP and the plasma potential Φ_{pl} simultaneously on the same position, by turning around equation (1) we can deduce the electron temperature T_{e}:

$$T_{\mathrm{e}} = \frac{\mathrm{e}(\Phi_{\mathrm{pl}} - V_{\mathrm{fl,cp}})}{\ln(|I_{\mathrm{es}}|/|I_{\mathrm{is}}|)}. \tag{5}$$

Drawing on equation (4) we can measure Φ_{pl} with an EEP. Therefore, if we have a CLP and an EEP nearby, we can determine T_{e} with a certain limited spatial resolution given by the distance between the two probes.

2.2. Robust strong EEPs for the NPH

In [13] also a detailed description of the robust, strong EEP to be used on the NPH is provided (see also [37, 39]). Here only a brief summary is given:

The greatest problem in constructing a sufficiently robust EEP, obviously being required to produce a strong emission current, was to find a material that, on one side, has a low

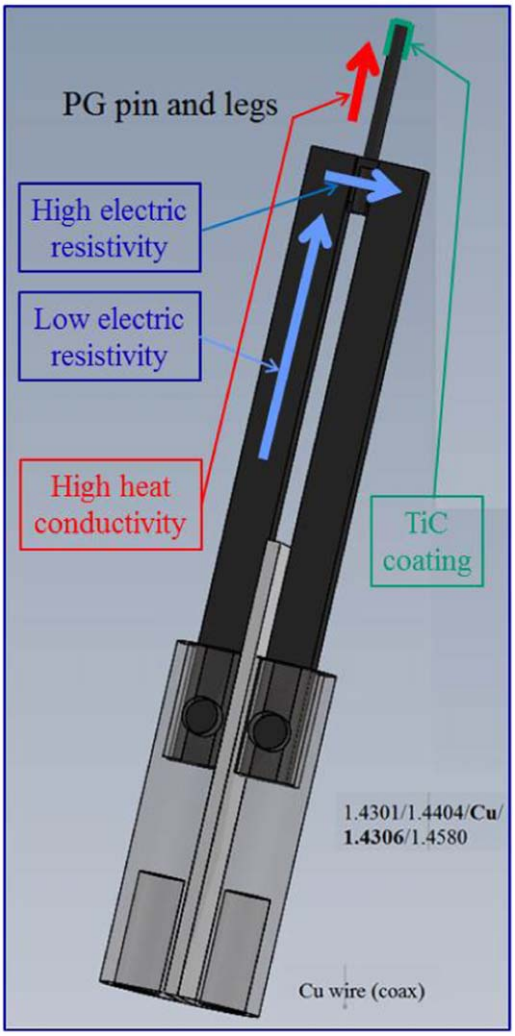

Figure 2. Schematic presentation of the EEP of highly oriented pyrolytic graphite (HOPG) for usage in the near SOL of MSTs. The blue arrows suggest the strongly different electric resistivity of HOPG in the two main directions of the graphite crystal lattice. The red arrow shows the direction of high heat conductivity from the HOPG 'loop' upward to the actual probe pin whose tip will be covered by a layer of titanium carbide. See also [13].

work function, guaranteeing a high emission current according to the law of Richardson and Dushman, while, on the other side, has to withstand the high plasma temperatures and particle fluxes in the SOL of a typical MST. In the deep SOL typical electron and ion temperatures can go up to 50 eV at densities of around 10^{19} m^{-3} and electron current densities up to 4×10^6 A m^{-2}.

Usually lanthanum hexaboride (LaB_6) would be considered as the best suited electron emitter for such purposes since it combines good chemical and thermal stability with a relatively low work function of 2.66 eV [40, 41]. For the purposes of an EEP to withstand the harsh conditions of a MST SOL, however, surprisingly it turned out that the melting and sublimation temperature of LaB_6 (2482 K) is too low. Our research showed that titanium carbide (TiC) will be better suited. Although it has a higher work function of 3.35 eV (thus producing lower electron emission for the same temperature as LaB_6), its far higher thermal stability than that of LaB_6 (up to 3420 K) compensates this disadvantage. See table 1 for a comparison between LaB_6 and TiC, including graphite and tungsten, the most frequently employed materials for an EEP in laboratory experiments. For further comparison this table also shows a typical current density $|j_{es}| - |j_{is}|$ (electron/ion saturation current density) in the deep SOL of an MST with $T_e \cong T_i = 50$ eV and a density of around 10^{19} m^{-3}. For a detailed discussion of this problem see [13].

The EEP for the NPH will therefore consist of a 1 mm diameter graphite pin coated with a thin film of TiC. Another important feature of the EEP is that it will be constructed of highly oriented pyrolytic graphite which will ensure that only the bridge between the two legs will be heated to the necessary temperatures for electron emission. More details of this EEP will be presented in our forthcoming paper [13].

Figure 2 shows a schematic presentation of the EEP that will be inserted into the NPH.

3. The NPH

3.1. The housing and shroud of the NPH

Graphite is the most favourite material for anything to be inserted into a hot plasma since it has a very high thermal stability (up to 4023 K) and is relatively insensitive to sputtering. Moreover, if sputtering occurs and carbon atoms enter the plasma, the relatively low atomic number of 6 keeps the Bremsstrahlung losses in an acceptable range. On the other hand, as mentioned above, sputtered-off graphite might deposit on other PFCs possible causing unwanted conductive layers.

Therefore the cylindrical shroud of the NPH for TCV, AUG, MAST-U and W 7-X, which encases the diagnostics, consists of graphite. The overall length of the probe is 208 mm, its diameter 25 mm. The latter dimension is determined by the maximum possible diameter of probe heads in TCV. The NPH carries on its top (right-hand side) two CLPs of pyrolytic graphite (PG) and one EEP also of PG, coated with TiC, as described in section 2.2. and shown in figure 2. Also on top there are two RFAs back to back, thus facing upstream and downstream. 40 mm behind the top two MPCs will be inserted into the NPH to record magnetic fluctuations in all three directions of space [21], on two radial positions. Figure 3 shows a schematic view of the entire NPH. For AUG a shroud of 50 mm diameter will be used for the NPH which will be coated by tungsten.

3.2. The diagnostics

The three probe pins of 1 mm diameter each and a protruding length of 3 mm consist of graphite and will be mounted in a row, slanted by 10° with respect to the total magnetic field in the edge region to avoid mutual shadowing. While the two outer probe pins will not be heated, thus acting as conventional CLPs, the centre pin will, as mentioned above, be

Table 1. Work functions W_w, real Richardson constants A^*, melting/sublimation points and densities of tungsten, graphite, lanthanum hexaboride and titanium carbide. The last row shows the values of the current density $|j_{es}| - |j_{is}|$ for an exemplary deep SOL of an MST ($T_e \cong T_i \cong 50$ eV and $n_{pl} \cong 10^{19}$ m^{-3}).

Substance	Work function, W_w (eV)	Richardson constant, A^* (A m^{-2} K^2)	Melting/sublimation point (K)	Density (kg m^{-3})	Highest theoretical emission at melting/sublimation point $j_{ep,max}$ (A m^{-2})
W	4.55	7.4×10^5	3695	19 300	6.37×10^6
C (graphite)	4.61	4.5×10^5	4023	2250	12.37×10^6
LaB_6	2.66	2.9×10^5	2482	4720	7.17×10^6
TiC	3.35	2.5×10^5	3420	4930	34.18×10^6
SOL plasma			$T_e \cong T_i \cong 50$ eV	$n_{pl} = 10^{19}$ m^{-3}	$\|j_{es}\| - \|j_{is}\| = 3.69 \times 10^6$ [13]

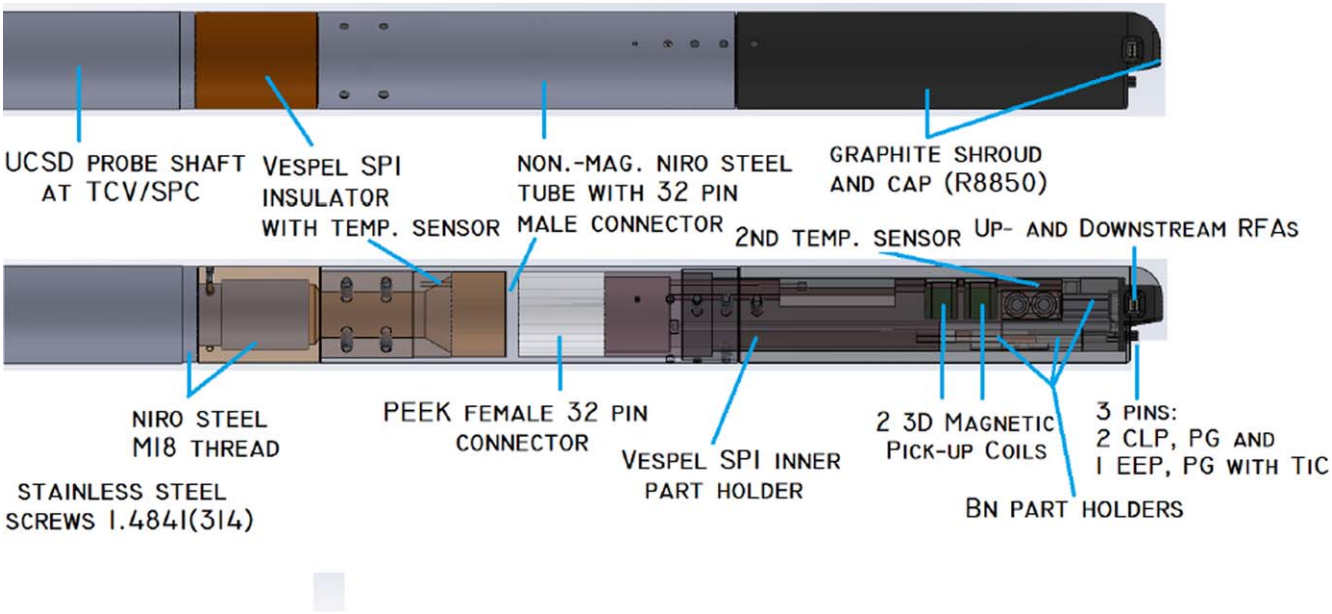

Figure 3. Schematic of the new probe head (NPH) for transport parameter measurements in the SOL of MSTs and W 7-X.

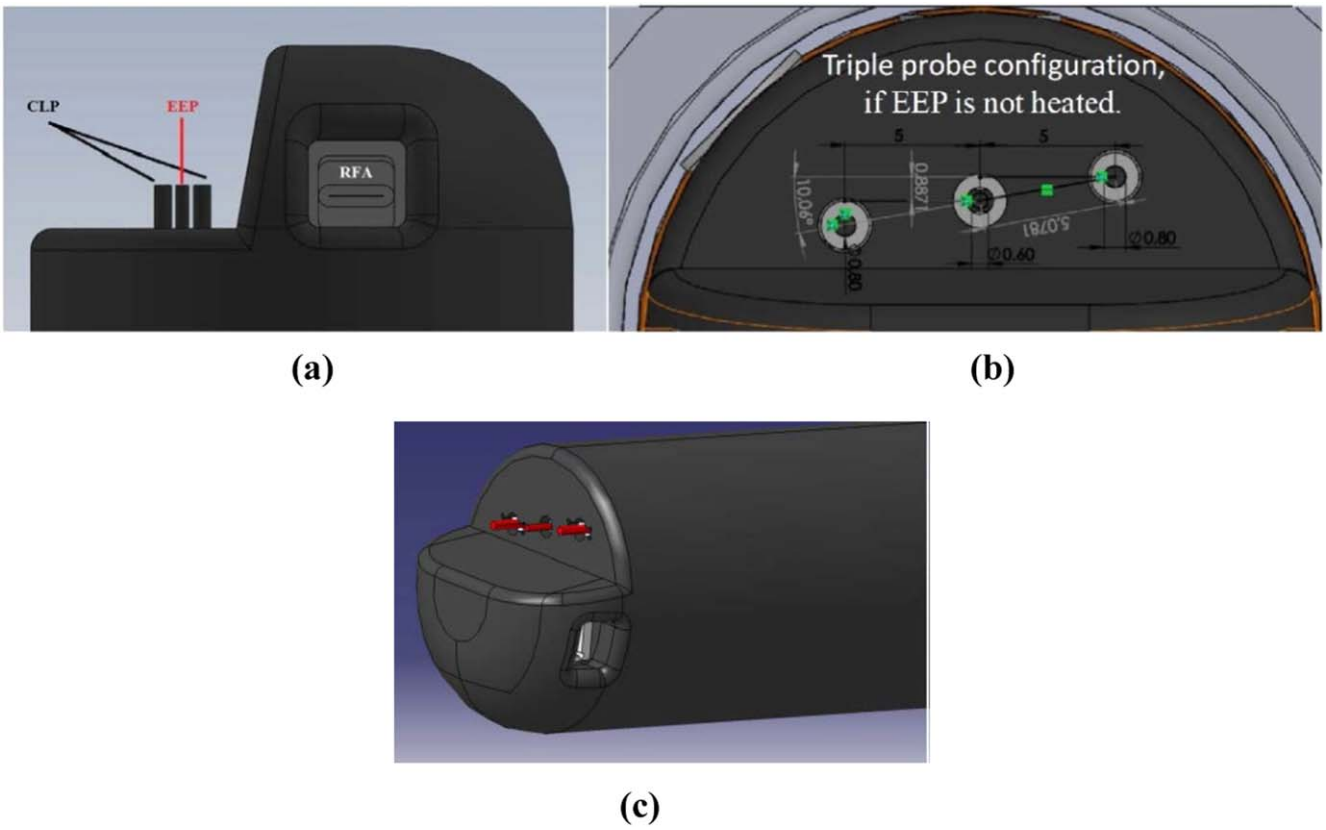

Figure 4. (a) Side view of the top of the NPH head along the magnetic field lines. The two CLP pins, the EEP pin and the RFA (up- and downstream) are positioned on the same radial position of a tokamak. (b) and (c) Views of the top of the NPH; the three pins are aligned along a line slanted with respect to the magnetic field to preventing shadowing effects. The centre pin is the EEP.

coated by TiC and heated externally (see section 2.2. and figure 2), thus acting as an EEP [13]. Figure 4 shows more details of the top of the NPH. Without heating the EEP the three probes can be used as triple probe for direct measurements of T_e [42].

3.2.1. Retarding field analysers (RFA). The two RFAs will be facing upstream and downstream to record the ion energy distributions [19], whereof the ion temperatures $T_{i,up}$ and $T_{i,down}$ can be deduced (see figure 5) [43]. The entrance slit of the RFAs has a width of 20–30 μm, the length of the slit is

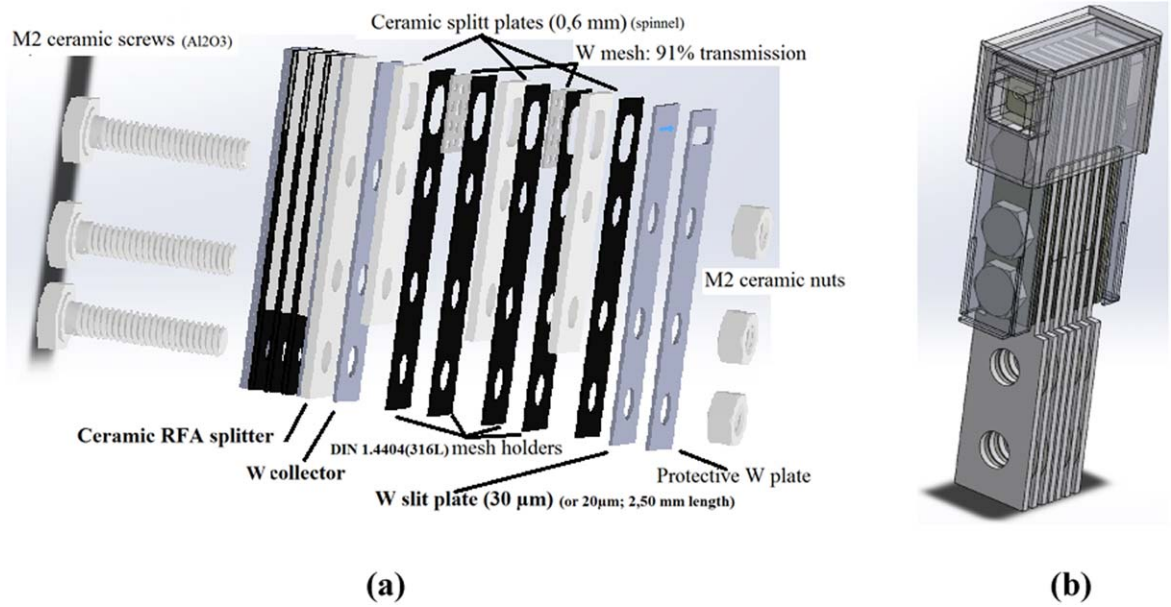

Figure 5. (a) The two RFAs, back to back; left hand side, assembled view; right hand side, exploded view. (b) The RFAs assembled.

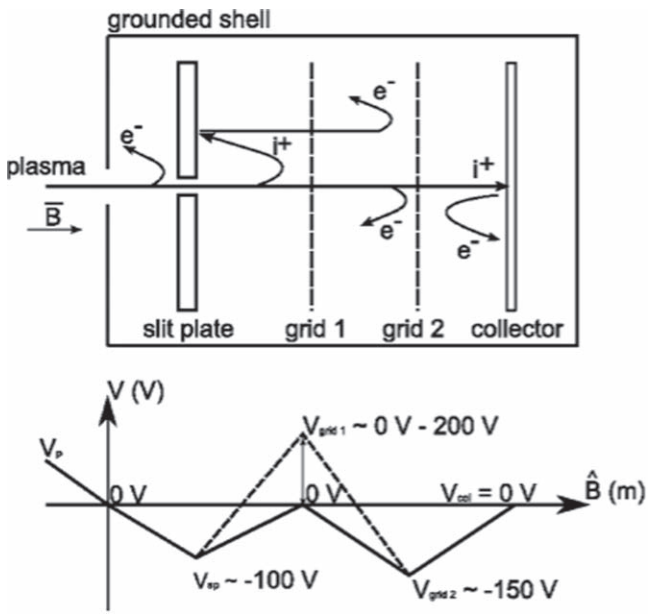

Figure 6. Example for the principle biasing scheme of a single RFA in ion-mode (the figure is taken from [43]).

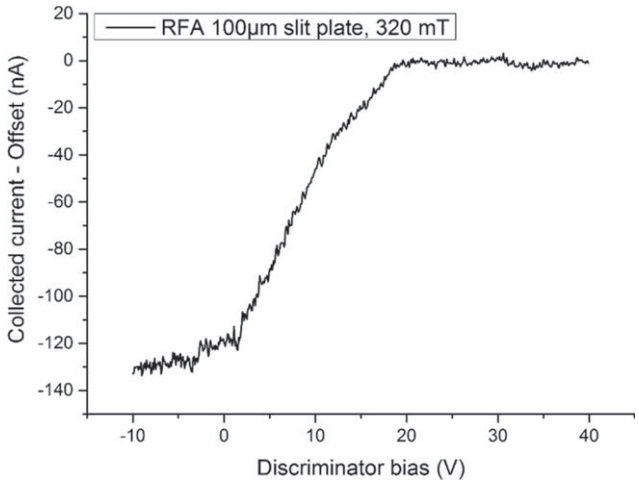

Figure 7. Test of a single RFA in the linear magnetic plasma device (LMPD) at the Jožef Stefan Institute in Ljubljana. The current is here shown in the technical current direction.

2.5 mm. The thickness of the tungsten slit plate is 0.1 mm. The expected transmission of the entire grid system is 0.5%.

The biasing scheme of the RFA grids is the usual one for recording the ion energy distribution, as shown for instance in figure 6 (from [43]). The negatively biased 'slit plate' repels the plasma electrons, the swept 'grid 1' is used to scan the energy distribution function of the ions. The negatively biased 'grid 2' repels secondary electrons released from the 'collector' by the impinging ions. Only about 0.5% of the plasma ions, gyrating along the magnetic field lines, arrive at the collector.

One prototype of such an RFA was tested in the linear magnetic plasma device (LMPD) at the Jožef Stefan Institute in Ljubljana at a magnetic field strength of 320 mT and a typical density of 10^{17} m^{-3} with $T_e \cong 3$ eV. The results showed that the actually measured current transmission (0.49%) agreed very well with the above-mentioned expected value.

Figure 7 shows an example of an ion energy distribution measured in the LMPD. From this characteristic we can deduce an ion temperature of about 0.2 eV. As assumed in table 1, in a typical MST SOL the temperatures will be $T_e \cong T_i \cong 50$ eV at a density of around 10^{19} m^{-3}. The expected ion current in a typical SOL will therefore be in the range of several tens of μA.

3.2.2. Magnetic pickup coils. The two MPCs will be contributed by the group at ENEA-RFX in Padua [21, 22]. Figure 8 shows a schematic of the two MPCs and a photo of

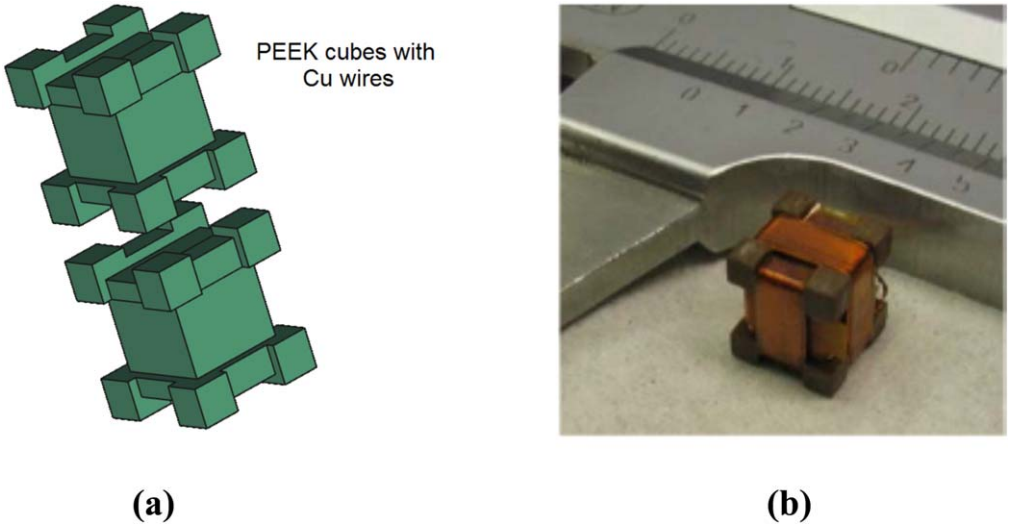

Figure 8. (a) Schematic of the two magnetic pickup coils (MPC) inserted into the NPH; (b) photo of one MPC with the dimensions $8 \times 8 \times 8$ mm^3.

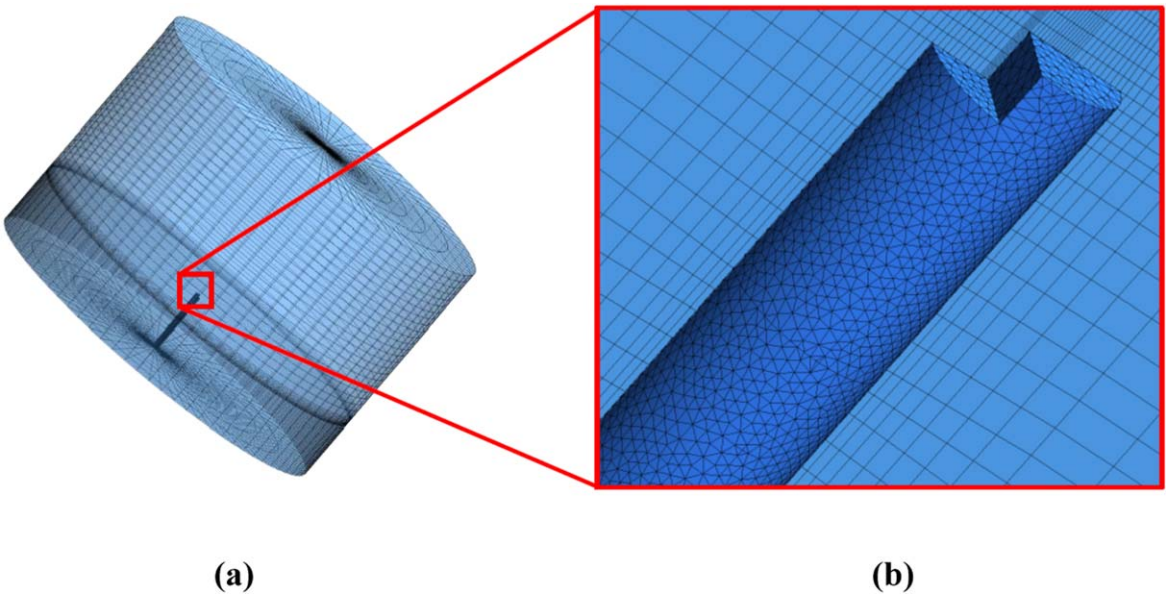

Figure 9. Simulation domain for NPH heat load simulations: (a) outside domain approximating the tokamak walls as a cylinder with a height of 1 m and a diameter of 1.5 m. (b) Mesh simulating the surface of the top graphite shroud of the NPH.

one coil for comparison with a scale. The corpus of such a triaxial MPC consists of PEEK® carrying three coils obtained by winding a 0.12 mm diameter wire around a small parallelepiped-shaped support ($8 \times 8 \times 8$ mm^3). The bandwidth for magnetic measurements is above 1 MHz with −3 dB cutoff at 1.1 MHz.

3.3. Heat-stress simulations

Since the NPH will be inserted into rather hot plasma its heat resistance had to be investigated. To this end heat flux and stress simulations have been carried out. A detailed description of the modelling approach with the simulation results is given in [44]. Here a few first results are summarised. Further results will be published in a later publication [45].

The NPH will be cooled to the outside only by thermal radiation. For the simulations the temperature of the outer radiating surfaces of the graphite shroud was set to 100 °C. The outside domain that should approximate the tokamak walls was modelled as a cylinder with a height of 1 m and a diameter of 1.5 m and a temperature of also 100 °C. The heat sink for the heat conduction represents the bottom surface of the metal shaft with a fixed temperature of 100 °C. The initial temperature of the probe at the start of the transient is also set to 100 °C. The probe and the outside space are meshed by the hybrid mesh consisting of 0.385 million tetra and hexa elements. The meshing of the NPH and the outside domain is shown in figure 9.

The problem was approached from two sides. First the heat transfer model for steady state was solved and then also

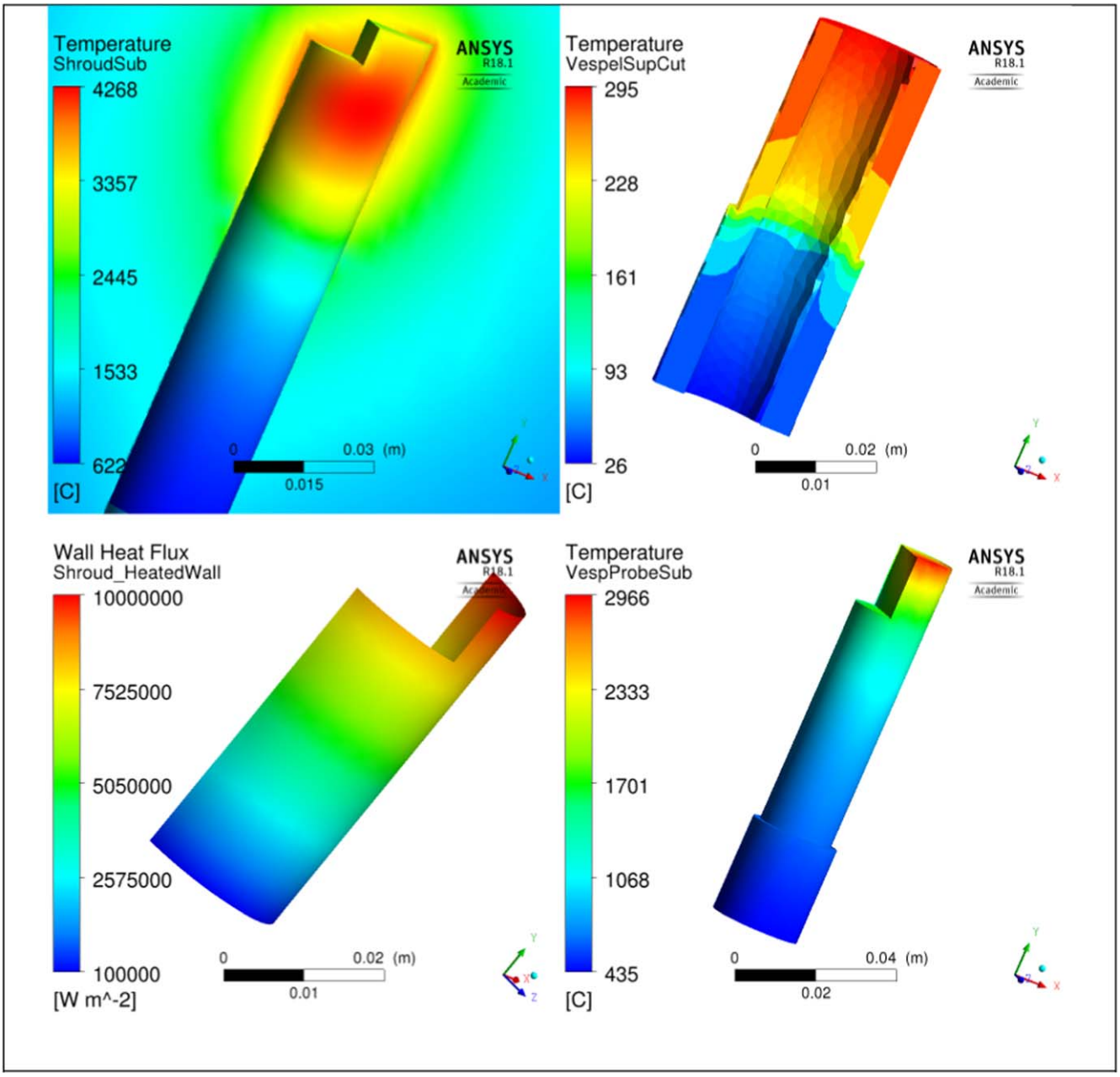

Figure 10. Results of the steady state simulation case: (top left) temperature distribution on the graphite shroud; (top right) temperature distribution along the cross-section of the supporting holder made of Vespel®; (bottom left) linear drop of the heat flux $q(x)$ from 10 to 0.1 MW m^{-2} applied on the upper 5 cm of the NPH shroud (bottom right) temperature distribution on the NPH inside Vespel® part.

transient heat load simulations were performed. Several simulation cases were carried out. Here two of them are presented:

3.3.1. Steady state simulation. First a steady state case with a linear axial distribution of isotropic heat flux $q(x)$ onto the NPH's shroud was assumed. Naturally this case is not very relevant since under no circumstances could any probe stay in the SOL during an entire discharge of an MST. Nevertheless, such a simulation can give us a first idea of the general behaviour of the NHP in the SOL of an MST. For this initial simulation a rather low value of $q(x) \cong 10$ MW m^{-2} was chosen on the top of the NPH, down to 0.1 MW m^{-2} at the lowest part of the shroud still immersed in plasma, which was estimated to be lying 5 cm lower. The solver balances between the heat source and the sinks with the residual target of 10^{-5} using auto-timescale. The results are presented in figure 10.

As can be seen in the top left graph in figure 10, the graphite shroud would reach temperatures above its sublimation point (around 4000 °C). However, even at such temperatures, the supporting holder made of VESPEL® SP1 would not heat to temperatures above 300 °C, as shown in the top right graph of figure 10. The parts made of VESPEL® are the most critical parts of the probe, as their temperature should stay below 300 °C (VESPEL® sublimation point)

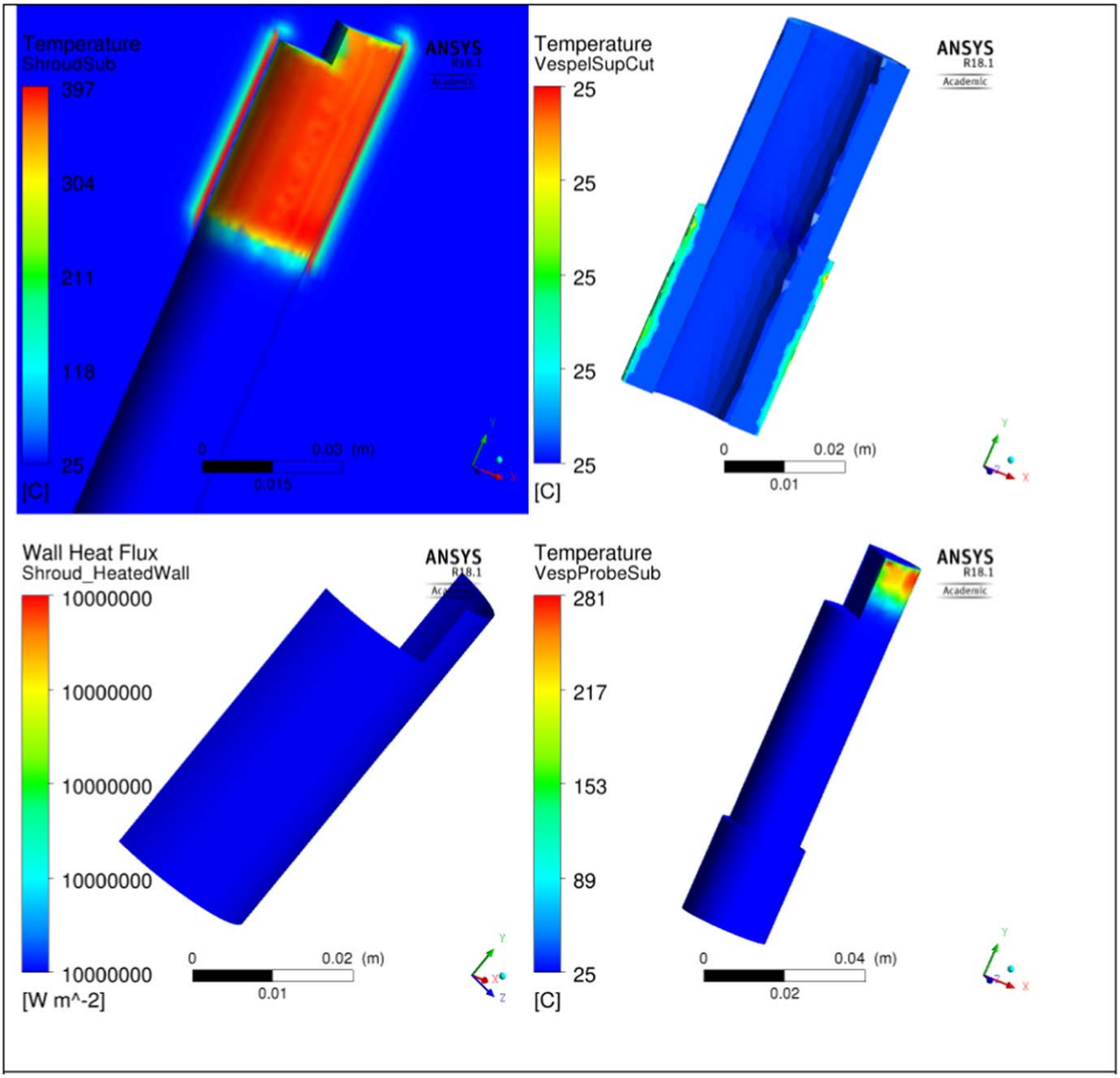

Figure 11. Results of the transient simulation case: (top left) temperature distribution on the graphite shroud; (top right) temperature distribution along the cross-section of the supporting holder; (bottom left) constant heat flux of 10 MW m^{-2} applied on the upper 5 cm of the NPH shroud (bottom right) temperature distribution on the NPH inside Vespel® part.

Table 2. List of plasma parameters to be determined simultaneously or comparatively with the NPH: $B_{r,p,t}$ radial, poloidal and toroidal magnetic field components. The third column shows the range of temporal resolution with which the parameters can be determined with the diagnostics of the NPH.

Diagnostic tool	Plasma parameter	Sampling rate
Two CLPs	V_{fl}, n_e	MHz
Swept CLP (I_p–V_p characteristic)	T_e, Φ_{pl}	kHz
EEP	$V_{fl} \simeq \Phi_{pl}$	MHz
One CLP & the EEP	T_e (equation (5))	MHz
Three CLPs (triple probe method with the EEP unheated [42])	T_e	MHz
Up- and downstream RFA (swept)	T_i, n_i	kHz
Two MPCs, 40 mm radially behind the top of the NPH	$\partial B_r/\partial t$, $\partial B_p/\partial t$, $\partial B_t/\partial t$,	MHz

during the probe exposure to hot plasma. This material is used in the NPH as a structural material in the supporting holder as well as an electrical insulation in the probe head. Below 300 °C, the VESPEL® material practically does not outgas and can be repeatedly heated up without losing its thermal or mechanical properties. The result in the top right of figure 10 shows that the supporting function of this VESPEL® part would not be compromised even for the case where the NPH would be stuck at a completely extended position. Nevertheless, as can be seen in the bottom right graph of figure 10, the inside VESPEL® part would reach temperatures much higher than 300 °C.

3.3.2. Transient case simulation. A more realistic case is of course the transient case, where the probe is only briefly exposed to heating from plasma for a short time. Here preliminary results of a simulation of a single plunge of the probe are presented, exposing it to plasma for 0.1 s. In this case a conservative assumption of the heat flow was used, being uniformly distributed along the top 5 cm of the NPH shroud of $q_0 = 10\ \mathrm{MW\,m^{-2}}$. The initial temperature of the NPH is set to 25 °C in this case. In the top right graph of figure 11 we see that the VESPEL® support would almost not heat up at all, while the bottom right graph shows that the inner VESPEL® part would stay below the critical temperature of 300 °C. The estimated temperature of the shroud after one plunge is assumed to not exceed 400 °C.

3.4. Possible measurements

As a summary, table 2 presents a list of plasma parameters which can be measured either simultaneously or with various methods for comparative purposes with the NPH. We would like to point out that the simultaneous determination of electron and ion temperature in the SOL would be especially relevant for getting a better insight into the formation and the propagation of blobs. Especially valuable will be that identical NPHs will be available at various MSTs, which will make it possible to directly analyse and compare the results and to draw generalised conclusions. At AUG, in particular, two NPHs will used simultaneously on the MEM and the XPR, thus in the toroidal mid plane and at the X-point, yielding new insights into the transport from the LFS mid plane towards the divertors.

In addition measurements with the NPH will also deliver valuable instruments to compare and benchmark the experimental data with the results of edge plasma simulations codes for mid plane transport such as the HESEL code [46].

4. Conclusion

We have developed a diagnostics tool for the measurement of various relevant plasma parameters in the edge region of toroidal fusion experiments. This is a probe head combining two CLPs, one EEP, two RFAs and two MPCs. Identical types of this probe head shall be used on three European MSTs and Wendelstein 7-X. We are confident that by comparative investigations we will be able to contribute to a better understanding of blobs, their origin and propagation through the edge region. We hope for a better insight into the problem of plasma losses across the magnetic field of toroidal fusion experiments.

Acknowledgments

This work has been carried out within the framework of the EUROfusion Consortium and has received funding from the EURATOM research and training programme 2014–2018 under Grant Agreement No. 633053. The views and opinions expressed herein do not necessarily reflect those of the European Commission. Bernd Schneider has been a fellow of the Friedrich Schiedel Foundation for Energy Technology. This work was also supported by the Commission for the Coordination of Nuclear Fusion Research in Austria (KKKÖ – Austrian Academy of Sciences), by the Tiroler Wissenschaftsförderung, by the Bilateral Scientific-Technical project SI 09/2016 between Austria and Slovenia, by the Slovenian research program Fusion technologies (P2-0405) and by the CEEPUS Network AT-0063.

ORCID iDs

C Ionita https://orcid.org/0000-0003-4875-6213
J J Rasmussen https://orcid.org/0000-0002-3543-690X
N Vianello https://orcid.org/0000-0003-4401-5346
R Schrittwieser https://orcid.org/0000-0002-6403-0511

References

[1] Ionita C *et al* 2018 New diagnostic tools for transport measurements in the scrape-off layers (SOL) of medium-size tokamaks (MST) *19th Int. Congress on Plasma Physics (ICPP 2018) (Vancouver, Canada, 4–8 June 2018)* (Topical Invited Lecture) (https://docs.google.com/document/d/1I1VFaC357x4mt2HT_bKqd8pW7f3k0GJrwNOmzL-7Gvw/edit)

[2] Myra J R, D'Ippolito D A, Stotler D P, Zweben S J, LeBlanc B P, Menard J E, Maqueda R J and Boedo J 2006 Blob birth and transport in the tokamak edge plasma: analysis of imaging data *Phys. Plasmas* **13** 092509

[3] Tsui C K *et al* 2018 Filamentary velocity scaling validation in the TCV Tokamak *Phys. Plasmas* **25** 072506

[4] Vianello N *et al* 2011 Direct observation of current in ELM filaments on ASDEX Upgrade *Phys. Rev. Lett.* **106** 125002

[5] Endler M 1999 Turbulent SOL transport in stellarators and Tokamaks *J. Nucl. Mater.* **266–269** 84–90

[6] van Milligen B P, Nicolau J H, Liu B, Grenfell G, Losada U, Carreras B A, García L, Hidalgo C and TJ-II Team 2018 Filaments in the edge confinement region of TJ-II *Nucl. Fusion* **58** 026030

[7] Kocsis G *et al* 2016 Investigation of edge filament dynamics in W7-X limiter plasmas *43rd EPS Conf. on Plasma Physics, European Conf. Abstracts* vol 40A *(Leuven, Belgium, 4–8 July 2016)* p 4.003 (http://ocs.ciemat.es/EPS2016PAP/pdf/P4.003.pdf)

[8] Mott-Smith H M and Langmuir I 1926 The theory of collectors in gaseous discharges *Phys. Rev.* **28** 727–63

[9] Langmuir I 1929 The interaction of electron and positive ion space charges in cathode sheaths *Phys. Rev.* **33** 954–89

[10] Schrittwieser R *et al* 2002 Measurements with an emissive probe in the CASTOR tokamak *Plasma Phys. Control. Fusion* **44** 567–78

[11] Ionita C *et al* 2011 The use of emissive probes in laboratory and tokamak plasmas *Contrib. Plasma Phys.* **51** 264–70

[12] Adámek J *et al* 2005 Comparative measurements of the plasma potential with the ball-pen and emissive probes on the CASTOR tokamak *Czech. J. Phys.* **55** 235–42

[13] Schneider B S *et al* Electron-emissive probe for investigations in hot plasmas in preparation

[14] Ionita C *et al* Plasma potential probes for hot plasmas *Eur. Phys. J.* D in print

[15] Sheehan J P and Hershkowitz N 2011 Emissive probes *Plasma Sources Sci. Technol.* **20** 063001

[16] Adámek J, Stöckel J, Hron M, Ryszawy J, Tichý M, Schrittwieser R, Ionita C, Balan P, Martines E and Van Oost G 2004 A novel approach to direct measurement of the plasma potential *Czech. J. Phys.* **54** C95–9

[17] Costea S, Fonda B, Kovacic J, Gyergyek T, Schneider B, Schrittwieser R and Ionita C 2016 Bunker probe: a plasma potential probe almost insensitive to its orientation with the magnetic field *Rev. Sci. Instrum.* **87** 053510

[18] Schneider B S *et al* 2016 Advanced probe for transport measurements in Medium-Size Tokamaks *29th Symp. on Fusion Technology (SOFT) (Prague, Czech Republic, 5–9 September 2016)* (Institute of Plasma Physics, Czech Academy of Sciences) p 716 Book of Abstracts

[19] Schneider B S *et al* 2017 Multi-diagnostic probe head for near-wall electric and magnetic measurements in Medium-Size Tokamaks *44th European Physical Society Conf. on Plasma Physics (Belfast, Northern Ireland, 26–30 June 2017)* p 4.105 (http://ocs.ciemat.es/EPS2017ABS/pdf/P4.105.pdf)

[20] Schneider B S *et al* 2018 Comparison of tokamak plasma mid-plane with divertor conditions and consequences for modelling *23rd Joint EU-US Transport Task Force Meeting (Sevilla, Spain, 11–14 September)* (http://psft.eu/ttf2018/wp-content/uploads/2018/09/ttf2018_full-program.pdf)

[21] Vianello N, Antoni V, Spada E, Spolaore M, Serianni G, Cavazzana R, Bergsåker H, Cecconello M and Drake J R 2005 Reynolds and Maxwell stress measurements in the reversed field pinch experiment extrap-T2R *Nucl. Fusion* **45** 761–6

[22] Spolaore M, Vianello N, Agostini M, Cavazzana R, Martines E, Scarin P, Serianni G, Spada E, Zuin M and Antoni V 2009 Direct measurement of current filament structures in a magnetic-confinement fusion device *Phys. Rev. Lett.* **102** 165001

[23] Hofmann F *et al* 1994 *Plasma Phys. Control. Fusion* **36** B277–87

[24] Herrmann A and Gruber O 2003 *Fusion Sci. Technol.* **44** 569–77

[25] Clery D 2015 *Science* **348** 854–6

[26] Klinger T *et al* 2013 Towards assembly completion and preparation of experimental campaigns of Wendelstein 7-X in the perspective of a path to a stellarator fusion power plant *Fusion Eng. Des.* **88** 461–5

[27] Ionita C *et al* 2013 Radial transport in the far SOL of ASDEX Upgrade during L-mode and ELMy H-mode *Nucl. Fusion* **53** 043021

[28] Ionita C *et al* 2009 Simultaneous measurements of electrostatic and magnetic fluctuations in ASDEX Upgrade edge plasma *J. Plasma Fusion Res. Ser.* **8** 413–8

[29] Watkins J G, Taussig D, Boivin R L, Mahdavi M A and Nygren R E 2008 High heat flux Langmuir probe array for the DIII-D divertor plates *Rev. Sci. Instrum.* **79** 10F125

[30] Adámek J, Horacek J, Seidl J, Müller H W, Schrittwieser R, Mehlmann F, Vondracek P, Ptak S and COMPASS and ASDEX Upgrade Team 2014 Direct plasma potential measurements by ball-pen probe and self-emitting Langmuir probe on COMPASS and ASDEX Upgrade *Contrib. Plasma Phys.* **54** 279–84

[31] Killer C, Drews P, Grulke O, Cai J, Henkel M, Knieps A, Li Y, Liu S, Nicolai D, Satheeswaran G and W7-X Team 2018 Characterization of the W7-X Scrape-Off Layer using the multipurpose manipulator *27th IAEA Fusion Energy Conf. (Ahmedabad, India, 22–27 October 2018)* (https://conferences.iaea.org/indico/event/151/papers/6247/files/4612-iaea_proceeding_killer.pdf)

[32] Langmuir I 1923 The pressure effect and other phenomena in gaseous discharges *J. Franklin Inst.* **196** 1–10
Also in Langmuir I 1961 *The Collected Works of Irving Langmuir* ed C Guy Suits vol 5 (Oxford: Pergamon) pp 1–10

[33] Schrittwieser R, Ionita C, Balan P, Silva C, Figueiredo H, Varandas C A F, Juul Rasmussen J and Naulin V 2008 Turbulence and transport measurements with cold and emissive probes in ISTTOK *Plasma Phys. Control. Fusion* **50** 055004

[34] Gyergyek T and Kovačič J 2013 Potential formation in a bounded plasma system which is terminated by an electron emitting floating collector studied by a particle-in-cell computer simulation *Contrib. Plasma Phys.* **53** 189–201

[35] Schrittwieser R *et al* 2008 Laser-heated emissive plasma probe *Rev. Sci. Instrum.* **79** 083508

[36] Schrittwieser R, Ionita C, Rahbarnia K, Gruenwald J, Windisch T, Stärz R, Grulke O and Klinger T 2013 Measurements of HF-plasma oscillations by means of a laser-heated emissive probe *Contrib. Plasma Phys.* **53** 92–5

[37] Schneider B S, Costea S, Ionita C, Schrittwieser R, Naulin V, Rasmussen J J, Stärz R, Vianello N, Kovacic J and Gyergyek T 2015 Indirectly heated strong and robust emissive probe for dense and hot plasmas *32th Int. Conf. Phenomena in Ionized Gases (ICPIG) (Iasi, Romania, 26–31 July 2015)* p 1.36 four-page extended abstracthttp://plasma.uaic.ro/icpig2015/Content/Posters/P1.36.pdf

[38] Campanell M D and Umansky M V 2016 Strongly emitting surfaces unable to float below plasma potential *Phys. Rev. Lett.* **116** 085003

[39] Schneider B S, Costea S, Ionita C, Schrittwieser R, Naulin V, Rasmussen J J, Stärz R, Vianello N, Kovacic J and Gyergyek T 2015 Robust highly emissive probe for plasma potential measurements in the edge region of toroidal plasmas *Proc. Sci.* electronic version (http://pos.sissa.it/archive/conferences/240/072/ECPD2015_072.pdf)

[40] Leung K N, Pincosy P A and Ehlers K W 1984 Directly heated lanthanum hexaboride filaments *Rev. Sci. Instrum.* **55** 1064–8

[41] Lafferty J M 1951 Boride cathodes *J. Appl. Phys.* **22** 299–309

[42] Chen S-L and Sekiguchi T 2004 Instantaneous direct-display system of plasma parameters by means of triple probe *J. Appl. Phys.* **36** 2363–75

[43] Elmore S *et al* 2012 Upstream and divertor ion temperature measurements on MAST by retarding field energy analyser *Plasma Phys. Control. Fusion* **54** 065001

[44] Končar B, Kovačič J, Draksler M and Schneider B 2018 Thermal analysis of MST probe exposed to fusion relevant SOL plasma *27th Int. Conf. Nuclear Energy of New Europe —NENE2018 (Portorož, Slovenia, 10–13 September 2018)* (Ljubljana: Nuclear Society of Slovenia) pp 604-1–604-9 oral contribution; Proc.

[45] Končar B *et al* Thermal analysis of MST probe exposed to fusion relevant SOL plasmain preparation

[46] Nielsen A H *et al* 2017 Numerical simulations of blobs with ion dynamics *Plasma Phys. Control. Fusion* **59** 025012